Yields of short-lived fission products produced following $^{235}U(n_{th},f)$

S. V. Tipnis, J. M. Campbell, G. P. Couchell, S. Li, H. V. Nguyen, D. J. Pullen, W. A. Schier, and E. H. Seabury
University of Massachusetts Lowell, Lowell, Massachusetts 01854

T. R. England
Los Alamos National Laboratory, Los Alamos, New Mexico 87545
(Received 15 July 1996; revised manuscript received 2 June 1997)

Measurements of gamma-ray spectra, following the thermal neutron fission of ^{235}U have been made using a high purity germanium detector at the University of Massachusetts Lowell (UML) Van de Graaff facility. The gamma spectra were measured at delay times ranging from 0.2 s to nearly 10 000 s following the rapid transfer of the fission fragments with a helium-jet system. On the basis of the known gamma transitions, forty isotopes have been identified and studied. By measuring the relative intensities of these transitions, the relative yields of the various precursor nuclides have been calculated. The results are compared with the recommended values listed in the ENDF/B-VI fission product data base (for the lifetimes and the relative yields) and those published in the Nuclear Data Sheets (for the beta branching ratios). This information is particularly useful for the cases of short-lived fission products with lifetimes of the order of fractions of a second or a few seconds. Independent yields of many of these isotopes have rather large uncertainties, some of which have been reduced by the present study. [S0556-2813(98)04106-5]

PACS number(s): 25.85.Ec, 29.30.Kv, 23.90.+w

I. INTRODUCTION

Independent (or direct) yields of fission products play an important role in the summation calculation approach towards the determination of decay heat. In this method, the total decay heat is estimated by adding up the beta and gamma yields from the individual nuclides. The method however requires an extensive data base of many hundreds of fission products that contribute in varying amounts to the total decay heat. The input for such calculations often comes from compilations like the ENDF/B-VI fission-product data base file, a comprehensive data file which has incorporated various experimental results as well as empirical model predictions of fission-product yields. This data base thus represents a good source of evaluated fission yield data. Since many fission-product nuclides lie quite far from the line of beta stability, their properties have not been completely determined [1], and the uncertainties associated with the production probabilities of many of these nuclides are quite large ($>60\%$ in some cases). This is especially the case when a nuclide has both a ground and metastable state or is short-lived (with a half-life of less than a few seconds). To overcome the incompleteness of these experimental data, current evaluations rely on nuclear models to supplement the experimental data base, or in some cases to replace the measurements if they have large uncertainties [2–5]. It has previously been shown that high-resolution gamma-ray spectroscopy can be used to accurately determine many fission-product yields [6–9]. The gamma-ray measurements for ^{235}U reported here are part of a larger study undertaken at the University of Massachusetts Lowell (UML), in collaboration with the Los Alamos National Laboratory (LANL), to measure the separate aggregate beta and gamma decay heats and gamma-ray spectra for ^{235}U, ^{238}U, and ^{239}U as a function of the delay time after fission. Our measurements of independent yields for delay times <20 s are of special importance since measured data from many short-lived nuclides are still missing. In this paper our measured independent and cumulative yields are compared with the current recommended values listed in the ENDF/B-VI fission product data base.

II. MEASUREMENTS

Measurements were carried out with the UML Van de Graaff accelerator which provides a proton beam impinging onto a thick lithium target (Fig. 1). The neutrons released in the $^{7}Li(p,n)^{7}Be$ reaction were moderated in paraffin blocks and vats of water surrounding the target. Thermal and epithermal neutrons induced fission in a thin foil of ^{235}U which lined the inside walls of a hemispherical fission cham-

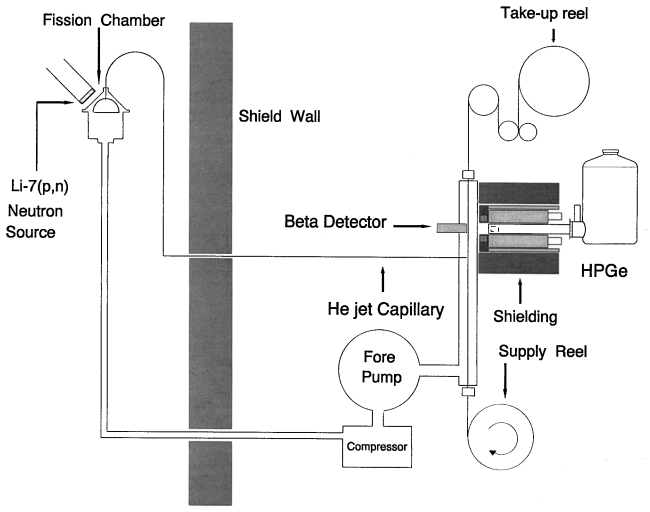

FIG. 1. Experimental arrangement at the UML Van de Graaff accelerator.

ber of radius 17 mm. In separate measurements it was shown that ~90% of the fission events were initiated by neutrons with energies below the ^{113}Cd capture resonance. Most of the remaining fission events are due to epithermal resonance neutrons with energies well below 1 keV, as it is estimated that for this source/moderator arrangement no more than 1–2 % of the fissions were due to fast neutrons. Since neutron-induced fission yields have only a weak energy dependence for incident-neutron energies below a few MeV, the measured yields represent essentially thermal neutron fission yields.

The fission chamber contained flowing helium gas saturated with oil vapor held at a pressure of four atmospheres (absolute). The size of the fission chamber and the operating pressure were chosen to give an essentially uniform transfer for fission fragments of all masses (i.e., light and heavy) [10]. A relative elemental transfer efficiency was determined by comparing the characteristic x rays produced by fission fragments escaping the fission foil at the source with their intensity at the catcher ''foil'' at the helium jet exit [11]. This study showed that the helium jet provided an almost uniform transfer efficiency for all fission-product elements with the possible exception of the noble gases krypton and xenon. Subsequent studies showed that even the noble gases were transported by the helium jet, but were not retained by the second-stage transport tape (see below). These results are consistent with an earlier study of a saturated-oil-vapor/helium-jet system by Feldstein and Amiel [12], which demonstrated a nearly uniform elemental transfer efficiency.

Fission fragments leaving the foil in the helium-jet fission chamber produce tracks of ionization which act as nucleation sites for the formation of microscopic oil droplets. The droplets with embedded fission fragments were transported very rapidly along the streamlines of helium through a capillary tube to a low background counting room. During the experiment, a 14-m long capillary was used for all but the very short delay times. For measurements at the short times a two-stage 2.9-m capillary was used. At the end of the capillary, the oil droplets with the fission fragments were sprayed onto a moving tape which transported the fragments to the detectors. (As noted above the noble gases krypton and xenon did not adhere to the transport tape and thus were lost. As a result, isotopes of these elements were not studied in this experiment.) The small size of the fission chamber resulted in rapid flushing and was a critical factor in maintaining the short transfer times. By varying both the tape speed and the detector distance from the spray point it was possible to measure aggregate gamma spectra over a large range of delay times.

The transport tape passed between a high purity germanium detector (HPGe) and a beta detector (a thin plastic scintillator, subtending a solid angle of almost 2π steradian to the tape). Spectra were measured at 17 delay times from 0.2 s to ~10 000 s (approximately 3 per time decade). Beta-gamma coincidence reduced the random background in the gamma spectrum and defined the part of the tape viewed, thus ensuring that the gamma spectrum was measured at a precise delay time interval. In addition, the germanium detector was surrounded by a NaI(Tl) annulus operated in an anticoincidence mode thus enabling measurement of Compton suppressed spectra. These delayed gamma spectra were recorded on a 4000 channel MCA, capable of measuring gammas from 80 keV to 5.5 MeV. In order to enhance the count rates in the experiment the HPGe detector was customized with a long snout, which allowed it to extend to the front face of the annulus (Fig. 2). Although this is not the optimum geometry for Compton suppression, considerable improvement in the background suppression was achieved, as is seen in Fig. 3. Typical background suppression factors were 1.7 (~0.5 MeV), 2.7 (~1.5 MeV), and 5.7 (~3.5 MeV). The improvement of the background at the high energy end was attributed in part to the rejection of cosmic rays by the annulus.

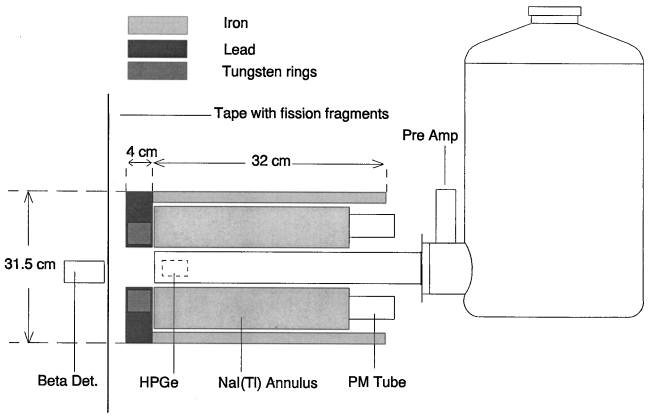

FIG. 2. Cross section of the HPGe detector with the NaI(Tl) annulus and associated shielding.

III. RESULTS AND ANALYSIS

Since the measurement of yields in this experiment was done on the basis of gamma line intensities, it was critical to

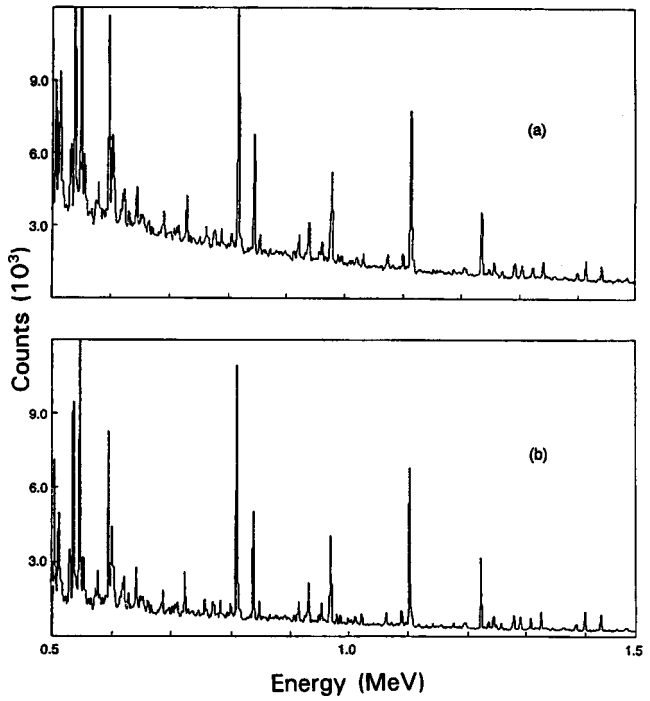

FIG. 3. Effect of the Compton suppression annulus. (a) Section of a typical Compton unsuppressed gamma spectrum (delay time: 1.484–2.191 s). (b) Same spectrum section as in (a), with Compton suppression.

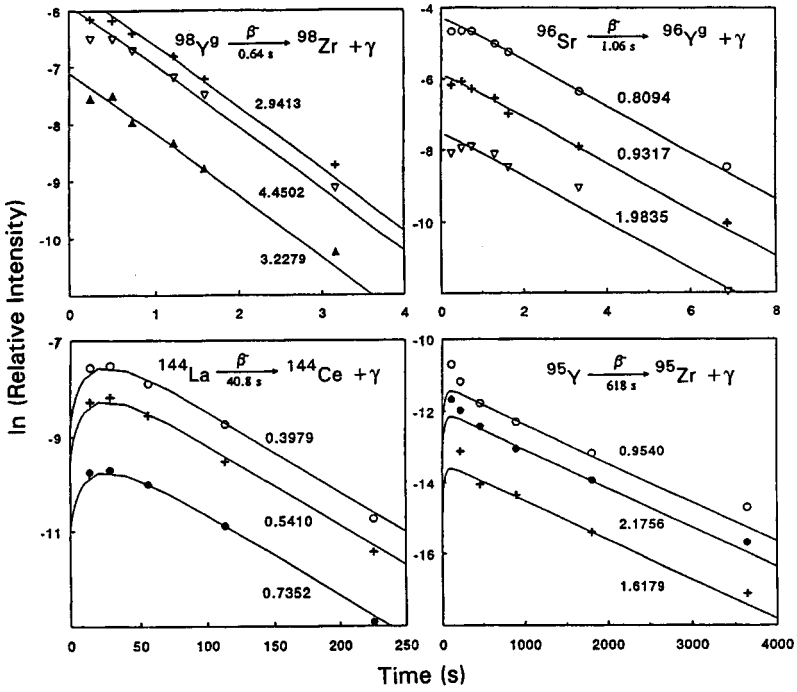

FIG. 4. Time evolution curves of the gamma lines for some specific isotopes. The abscissa corresponds to the delay time in seconds and the ordinate to the natural logarithm of the relative intensities of the lines. Energies in MeV of the individual gamma lines are shown in each case.

identify correctly the parent nuclide which produced a given gamma line. By measuring fission-product gamma spectra at many delay-time intervals after fission, sensitivity to a particular nuclide was maximized for spectra measured at delay times roughly matching the nuclide lifetime. For example in a spectrum measured at a delay time of 10.0–12.0 s, isotopes with half-lives of a few seconds would have decayed away considerably by the time they reached the detector and would not make a significant contribution. On the other hand, isotopes whose half-lives were of the order of many tens of seconds or longer would not decay significantly over such a short time interval. The measured gamma spectrum thus has lines mainly from the daughters of those isotopes whose half-life matched the delay time interval. By following the time evolution of the intensities of the lines through several consecutive delay time spectra it was possible in most instances to determine whether the line was due to a single isotope or was an admixture due to two or more isotopes with lines at approximately the same energy. A second criterion used in establishing the purity of a particular gamma line was its relative intensity. Comparing the experimental relative intensities of lines to those listed in the Nuclear Data sheets (NDS), allowed us to further confirm that the lines were indeed due to a single isotope. This second criterion was particularly useful if a certain line had contributions from multiple species having roughly the same half-life. In this case the measured relative intensities would not match the ones from NDS. This two-pronged approach of examining the time-evolution of the intensities and their relative strengths helped us identify the source species of the gamma lines while assuring that lines used to determine the yields were not admixtures from two or more species.

Figure 3 shows a portion of a typical measured spectrum, with and without the Compton suppression. The energy resolution of the photopeaks (FWHM) in the spectra varied from 1.5 keV at 0.5 MeV to 4.25 keV at 4.5 MeV. Peak intensities and relative time normalization between successive delay times were calculated in the following way. The number of counts in each peak were corrected for the detector efficiency as a function of energy, and then divided by the total area of the spectrum. From a graph of the total gamma activity as a function of time, which was calculated by the program CINDER10 [13,14] using ENDF/B-VI data for $^{235}\mathrm{U}(n_{\mathrm{th}},f)$, the average gamma power was calculated for each of the experimentally measured delay time intervals. This factor was multiplied by the aforementioned ratio to account for the relative time normalization between the delay time intervals considering that the average gamma power varied from one interval to the next. The assumption here was that the total area of the spectrum follows the same time behavior as the activity versus time curve.

The normalized gamma yields were plotted on a logarithmic scale (ordinate) as a function of the delay times (abscissa). For each nuclide, a CINDER10 calculation of the beta activity of the parent species under investigation was fitted to these gamma yield data to check for the proper time behavior and to obtain their relative intensities. Only those gamma lines which exhibited the proper time behavior were used in the fission-product yield analysis.

In most of the cases that were studied, the parent nuclide was found to be short-lived compared to the daughter so that the half-life of the daughter could be established from the slope of the decaying part of the logarithmic curve. Examples of these curves are shown in Fig. 4. The half-life measurements were useful in checking the assigned values in the ENDF/B-VI data base. It was found early on, for example, that the values of the measured lifetimes for $^{98}\mathrm{Y}^{m}$ and $^{98}\mathrm{Y}^{g}$ did not match the values calculated from the pre-

TABLE I. Comparison of relative intensities of gamma lines of ^{97}Y following the decay $^{97}\mathrm{Sr} \xrightarrow[(t_{1/2}=0.42\ \mathrm{s})]{} {}^{97}\mathrm{Y} + e^- + \overline{\nu}_e$.

Energy (MeV)	Relative intensities[a]	
	NDS	Measured
0.3071	11.20	16.4
0.6522	12.74	12.8
0.6973	6.80	7.0
0.8016	5.88	6.3
0.9538	23.91	24.7
1.9050	28.00	22.4
2.2120	10.78	9.7

[a]Intensity numbers are per 100 beta decays of the parent.

ENDF/B-VI beta activity plots for that nuclide, presumably due to a data entry error in this preliminary version of the compilation. The half lives of those two states were subsequently reversed in the ENDF/B-VI beta activity data to reflect the proper time dependence.

From the logarithmic plots of the normalized gamma yield versus time, the relative intensities of various gamma transitions of a given isotope were calculated. The sum of the experimental intensities was normalized to the corresponding sum from NDS, which lists the absolute intensities per 100 decays of the parent. As an example, Table I lists the measured and NDS intensities of the gamma lines associated with the beta decay of ^{97}Sr. From our measured values of the gamma intensities, the beta activity was then calculated for each parent. Only those transitions whose experimental relative intensities agreed well with the published values were chosen for this purpose. On average about four lines were chosen per isotope, typically in the energy range of 500 keV to 3.5 MeV. Lines with energies less than 200 keV were not used in the analysis since their intensities were often subject to ambiguity. This is because the low energy region of the spectra had a large number of gamma lines from different isotopes overlapping with each other thus making it difficult to identify their source species. Table II lists the gamma lines and the normalized intensities used in the analysis for each isotope.

For the case where the half-life of the parent nuclide is short compared to that of the daughter, which in turn is short lived compared to the granddaughter, the solutions of the Bateman equations for long times can be approximated by the form shown in Eq. (1), where the N's are the yields, subscripts 1, 2, and 3 denote the parent, daughter and granddaughter respectively and the subscript 0 denotes the independent yield of the nuclide, i.e., the primary yield of the nuclide following fission, after

$$N_3(t) \cong \left[N_{30} + b_2 \frac{\lambda_2 N_{20}}{(\lambda_2 - \lambda_3)} + b_1 \frac{\lambda_1 \lambda_2 N_{10}}{(\lambda_1 - \lambda_3)(\lambda_2 - \lambda_3)} \right] e^{-\lambda_3 t} \tag{1}$$

the emission of prompt neutrons. Thus the independent yield does not include any contribution from the beta decay of the precursor nuclides in the chain. The λ_i's are the decay constants and the b_i's are the branching ratios.

This approximation is indeed valid for most of the fission product chains that we studied. To estimate the independent yield of, say, the granddaughter, one has to subtract off the second and the third terms on the right hand side of Eq. (1). This means that the independent yield of the precursors must be known. In those cases, where the independent yields of the precursors could not be measured experimentally (typically when the yield was $<0.5\%$), the independent yield value from ENDF/B-VI has been used in Eq. (1) to estimate the independent yields of the daughter and/or the granddaughter. The cumulative yields for all the isotopes were calculated using the following equation:

$$N_3 = N_{30} + b_2 N_{20} + b_1 N_{10}. \tag{2}$$

Factors contributing to the uncertainties in the experimental values of isotopic yields were peak-stripping, detector efficiency, curve fitting of the beta activity on the time-evolution plots and the uncertainty in the beta branch values used in the analysis.

The uncertainty due to peak-stripping varied, depending on the energy and the intensity of the gamma line. Typical values ranged from 2% to 8%, with some high energy/low intensity lines having a value of 10%. A fixed value of 10% was taken for the combined effect of the first two factors (peak-stripping and detector efficiency). In the low-energy (high background) region, the detector efficiency was well-known, whereas in the high energy region (efficiency not quite as well-known) the background was very low. The two effects thus tended to compensate one another throughout the entire energy region of interest. In fact the value of 10% may be an overestimation in many cases.

The intensity of the gamma line was evaluated only after fitting the beta activity curve to 3 to 5 data points on the time-evolution plot. The measured intensity of the line was thus an average value, over several lifetimes of the parent nuclide. This process of following the gamma line through several delay times significantly reduced the uncertainty in its intensity. Uncertainty due to fitting the beta activity was taken to be 5%.

The beta branch uncertainty varied in each case depending on how well the spectroscopic information was documented in the NDS. The values varied from a few percent in some cases to as high as 30% in others and was the major source of experimental uncertainty in the latter cases. The net uncertainty for each nuclide was calculated by adding the individual contributions in quadrature.

To reduce the possibility of error due to overlap of gamma lines of the same energy, the yields were calculated on the basis of multiple gamma lines for each isotope, and only after making sure that they all exhibited the proper time evolution and relative intensities.

IV. DISCUSSION

Independent yields

Table III lists our values of the experimental independent yields along with the values assigned by the ENDF/B-VI fission product database as well as those measured by the Studsvik group of Rudstam *et al.* [9]. The latter set does not list independent yields of Y, Zr, Ba, and La presumably be-

TABLE II. Gamma lines and their intensities used in the determination of independent yields (energies and intensities are NDS values as presented in Refs. [15,18,20,21]).

Isotope	$t_{1/2}$	γ center (MeV) [% γ branch]				
^{89}Rb	15.2 m	1.0315 [54.0]	1.2485 [48.9]	2.1959 [12.0]	2.5702 [8.90]	
^{90}Rb^{g}	2.55 m	3.3830 [4.70]	3.5340 [2.80]			
^{90}Rb^{m}	4.3 m	1.3753 [16.4]	2.7526 [14.8]	3.3171 [12.7]		
^{91}Rb	58.4 s	1.8492 [4.13]	1.9709 [8.32]	2.5641 [11.3]	3.5996 [9.20]	4.0780 [3.13]
		2.5059 [1.60]	2.9257 [2.39]	3.4465 [1.45]		
^{92}Rb[a]	4.5 s	0.8149 [3.56]	1.7123 [0.65]	2.8200 [1.07]		
^{93}Rb	5.7 s	0.4236 [18.1]	0.7099 [6.65]	0.9861 [5.45]	1.3852 [6.02]	3.4582 [3.65]
^{93}Sr	7.42 m	0.3775 [1.90]	0.4465 [2.30]	0.7104 [20.6]	0.8755 [25.2]	0.8885 [20.6]
		1.2694 [9.30]	1.6942 [2.90]	1.6989 [3.80]	1.8115 [1.90]	2.2300 [1.50]
		2.3650 [2.30]				
^{94}Rb	2.7 s	0.8369 [87.3]	1.0894 [18.5]	1.3091 [13.7]	1.5775 [30.5]	
^{94}Sr	1.25 m	0.6217 [3.40]	0.8060 [2.07]	1.4277 [92.4]		
^{95}Rb	0.38 s	0.3287 [6.81]	1.4392 [4.56]	2.7986 [5.58]	3.2536 [2.51]	
^{95}Sr	25.1 s	0.6856 [20.3]	2.2476 [4.32]	2.7173 [4.77]	2.3310 [3.91]	
^{96}Sr	1.06 s	0.1223 [88.9]	0.2794 [8.75]	0.8094 [58.5]	0.9317 [11.8]	1.9836 [2.38]
^{96}Y^{m}	9.6 s	0.1467 [31.5]	0.6171 [57.9]	0.9145 [57.9]	1.1072 [46.9]	0.3633 [21.7]
		1.7506 [92.6]				
^{97}Sr	0.42 s	0.3071 [16.4]	0.6522 [12.8]	0.8016 [6.34]	0.9538 [24.7]	1.9050 [22.4]
		2.2120 [9.67]				
^{97}Y^{g}	3.5 s	1.9966 [9.76]	2.7430 [5.63]	3.2877 [16.9]	3.4017 [13.8]	
^{97}Y^{m}	1.23 s	0.9701 [39.4]	1.2442 [7.94]			
^{98}Y^{g}	0.64 s	2.4206 [4.53]	2.9413 [16.6]	3.2279 [3.53]	4.4502 [11.7]	
^{99}Y	1.47 s	0.5754 [10.2]	0.6140 [5.57]	0.7243 [18.5]	0.7822 [6.48]	
^{99}Zr	2.1 s	0.3872 [10.5]	0.4151 [5.23]	0.4617 [12.2]	0.4691 [54.9]	0.5461 [44.9]
		0.5940 [27.2]				
^{99}Nb^{m}	2.6 m	2.6413 [3.39]	2.8515 [2.44]			
^{100}Y^{g}	0.74 s	2.5150 [6.29]	2.846 [4.43]			
^{100}Zr	7.1 s	0.4005 [18.2]	0.4980 [1.22]	0.5043 [31.5]		
^{101}Zr	2.1 s	0.2056 [5.50]	1.8383 [1.66]	1.9570 [3.02]	2.0090 [2.55]	
^{102}Zr	2.9 s	0.5996 [13.9]				
^{136}I^{g}	1.39 m	1.9622 [2.17]	2.4146 [6.85]	3.1411 [0.759]		
^{136}I^{m}	46.9 s	0.3698 [11.7]	0.7501 [7.83]			
^{140}Cs	1.06 m	0.6023 [48.5]	0.9084 [8.87]	1.8533 [2.81]	2.1016 [2.54]	2.5219 [2.54]
^{141}Cs	24.9 s	0.5551 [3.53]	0.6920 [3.19]			
^{141}Ba	18.27 m	0.1903 [47.9]	0.2769 [26.3]	0.3040 [15.2]	0.3430 [15.2]	0.4670 [7.20]
		0.6470 [7.90]	0.7390 [4.60]	1.1975 [5.90]	1.6820 [3.20]	
^{142}Cs	1.7 s	0.3596 [25.3]	0.9669 [12.0]	1.1759 [3.43]	1.3265 [12.6]	
^{142}Ba	10.6 m	0.2553 [18.6]	0.8952 [13.3]	0.9491 [11.8]	1.0012 [7.69]	1.0787 [9.98]
		1.2043 [17.0]				
^{143}Cs	1.78 s	0.6617+0.6599 [8.36]		0.2630 [3.68]	0.2324 [10.5]	0.1955 [14.9]
^{143}Ba	14.5 s	0.2115 [24.3]	0.7987 [16.3]	1.0107 [8.51]		
^{143}La	14.1 m	0.7981 [1.18]	1.5560 [1.02]	1.9610 [0.92]	2.5000 [0.79]	
^{144}Ba	11.4 s	0.1565 [12.7]	0.2285 [1.94]	0.3885 [14.3]	0.4305 [19.3]	
^{144}La	40.9 s	0.5842 [10.2]	0.5410 [35.7]	0.7352 [8.37]	0.8447 [18.6]	1.4317 [6.85]
		2.0084 [2.06]				
^{145}Ba	4.31 s	0.3032 [3.02]	0.3252 [2.13]	0.3788 [4.29]		
^{145}La	24.8 s	0.3558 [3.97]	0.4474 [3.59]	0.6718 [1.70]	0.9320 [2.79]	1.8195 [2.79]
		2.1555 [1.19]	2.3594 [1.08]	2.3771 [0.66]		
^{146}La	6.27 s	0.7023 [6.72]	0.9246 [6.72]	1.4980 [2.02]	2.6940 [0.96]	
^{147}La	4.4 s	0.1860 [5.98]	0.2360 [2.97]			

[a]Branching ratios normalized to values listed in [9] instead of NDS. See text for full explanation.

TABLE III. Comparison of independent yields (and their percentage uncertainty).

Isotope	$t_{1/2}$	ENDF	Expt.	Rudstam	Expt./ENDF	Expt./Rudstam
^{89}Rb	15.2 m	0.20 (11)	0.91 (14)	1.17 (9)	4.6 (18)	0.78 (17)
^{90}Rb^{g}	2.55 m	0.139 (6)	0.61 (15)	0.43 (16)	4.3 (16)	1.42 (22)
^{90}Rb^{m}	4.3 m	0.71 (>64)	1.6 (12)	0.59 (12)	2.2 (>65)	2.7 (17)
^{91}Rb	58.4 s	2.225 (1.4)	2.9 (13)	2.24 (2)	1.30 (13)	1.29 (13)
^{92}Rb[c]	4.5 s	3.132 (2)	5.7 (38)	2.75 (11)	1.8 (38)	2.1 (40)
^{93}Rb	5.7 s	3.067 (1.4)	3.3 (13)	2.95 (8)	1.08 (13)	1.12 (15)
^{93}Sr	7.42 m	2.570 (2)	2.1 (35)	1.98 (21)	0.8 (35)	1.1 (41)
^{94}Rb	2.7 s	1.567 (3)	1.17 (11)	1.24 (9)	0.75 (12)	0.94 (14)
^{94}Sr	1.25 m	4.513 (1.4)	4.6 (14)	4.7 (15)	1.02 (14)	0.98 (21)
^{95}Rb	0.38 s	0.764 (4)	0.69 (13)	0.71 (7)	0.90 (14)	0.97 (15)
^{95}Sr	25.1 s	4.538 (2)	5.3 (14)	4.51 (2)	1.17 (14)	1.18 (14)
^{96}Sr	1.06 s	3.568 (2)	2.5 (13)	3.63 (2)	0.70 (13)	0.69 (13)
^{96}Y^{m}	9.6 s	2.02 (32)	0.94 (11)		0.47 (34)	
^{97}Sr	0.42 s	1.721 (3)	0.81 (14)	2.58 (21)	0.47 (14)	0.31 (25)
^{97}Y^{g}	3.5 s	3.14 (32)	1.4 (25)		1.1[a] (34)	
^{97}Y^{m}	1.23 s		2.0 (13)			
^{98}Y^{g}	0.64 s	1.11 (32)	1.4 (13)		1.3 (35)	
^{98}Y^{m}	2.0 s	1.11 (32)	0.8[b] (43)		0.7 (54)	
^{99}Y	1.47 s	1.950 (6)	1.2 (19)		0.62 (20)	
^{99}Zr	2.1 s	3.58 (23)	3.3 (28)		0.92 (36)	
^{99}Nb^{m}	2.6 m	0.407 (8)	5.0 (19)		12.3 (21)	
^{100}Y^{g}	0.74 s	0.61 (>64)	0.24 (22)		0.39 (>68)	
^{100}Zr	7.1 s	4.98 (32)	4.1 (16)		0.82 (36)	
^{101}Zr	2.1 s	2.788 (4)	2.8 (12)		1.01 (13)	
^{102}Zr	2.9 s	1.782 (4)	3.9 (12)		2.19 (13)	
^{136}I^{g}	1.39 m	1.320 (8)	1.2 (29)	0.29 (83)	0.91 (30)	4.1 (88)
^{136}I^{m}	46.9 s	1.251 (6)	1.07 (15)	1.09 (11)	0.86 (16)	0.98 (19)
^{140}Cs	1.06 m	2.070 (3)	2.6 (13)	2.4 (25)	1.26 (13)	1.1 (28)
^{141}Cs	24.9 s	2.915 (2)	4.3 (13)	3.11 (3)	1.48 (13)	1.38 (13)
^{141}Ba	18.27 m	1.66 (11)	1.7 (57)		1.0 (58)	
^{142}Cs	1.7 s	2.278 (4)	2.2 (15)	2.23 (17)	0.97 (16)	0.99 (23)
^{142}Ba	10.6 m	3.014 (6)	3.7 (21)		1.23 (22)	
^{143}Cs	1.78 s	1.403 (4)	1.3 (19)		0.93 (20)	
^{143}Ba	14.5 s	4.101 (4)	3.4 (24)	6.1 (13)	0.83 (24)	0.56 (27)
^{143}La	14.1 m	0.38 (>64)	2.9 (51)		7.6 (>82)	
^{144}Ba	11.4 s	3.975 (3)	4.0 (16)	3.93 (1)	1.01 (16)	1.02 (16)
^{144}La	40.9 s	1.070 (6)	0.4 (325)		0.4 (325)	
^{145}Ba	4.31 s	1.866 (6)	1.8 (17)	2.25 (25)	0.96 (18)	0.80 (30)
^{145}La	24.8 s	1.915 (8)	3.8 (35)		2.0 (36)	
^{146}La	6.27 s	1.490 (8)	1.3 (25)		0.87 (26)	
^{147}La	4.4 s	0.64 (11)	1.6 (20)		2.5 (23)	

[a]Metastable and ground state yields added up since ENDF/B-VI does not list the metastable state contribution.

[b]Estimated from charge-mass complementarity (see text).

[c]Yield based on gamma line intensities as listed in [9]. See text for full explanation.

cause of the lack of efficiency of the high temperature target-ion source for these elements. The data set is included here since it is useful to compare our yields to those determined from a different experiment. Percent uncertainties in the data are indicated in parentheses. The ENDF/B-VI yields are based on both experimental measurements and from predictions of the Z_p model of Wahl [15], an empirical model which describes a Gaussian dispersion of the independent elemental yields about a most probable atomic number Z_p for a constant atomic number A. Another empirical model, by the same author, called the A_p' model describes a Gaussian dispersion of atomic mass yields about the most probable value A_p' for a constant atomic number Z. In both models, the Gaussian distribution is modulated by the effect of even (odd) number of neutrons and protons which can affect the yields.

The level of agreement between the present results and the ENDF/B-VI recommended values as well as those of Rudstam *et al.* can be seen from the columns in Table III which list the ratios of the two values for each isotope. The

overall agreement is quite good. Barring cases where either the ENDF or the experimental uncertainties are $>60\%$, a comparison of the ratio of the yields reveals that 56% of the measured independent yields agree with the ENDF values within 1σ and 69% agree within 2σ, where σ is the combined uncertainty of the ratios.

For the case where the nuclide is formed in both the metastable and ground state, ENDF/B-VI does not have a reliable way of splitting the independent yield in the proper ratio. The problem arises due to the fact that in many such cases, experimental results for the isomeric yields are not well known. Model calculations predict only the total yield (metastable+independent) of each isotope and not the individual contributions of the two isomers. Thus in such cases the total yield of the nuclide as quoted by ENDF is a more reliable value than the individual yields of the isomeric and ground states. Some specific cases of disagreement and the possible reasons are now discussed.

For $^{90}Rb^m$ three gamma transitions were used in the analysis, all with energies above 1 MeV. Agreement with the NDS relative intensities and the time evolution curves were good in each case. However, our value for the independent yield of $^{90}Rb^m$ is considerably higher than the equivalent ENDF value. For this case NDS quotes a value of 0% for the ground state beta decay branch of $^{90}Rb^m$. Moreover since the decay of $^{90}Rb^m$ has $Q_{\beta^-}=6.589$ MeV, it is plausible that unreported transitions from higher energy states could increase our determined value of its independent yield even further. Also, it should be noted that ENDF assigns an uncertainty of $>64\%$ for the quoted value of the independent yield. In light of the above argument we feel that the ENDF assignment may be too low for $^{90}Rb^m$. Our value for the independent yield of $^{90}Rb^g$ is also high relative to ENDF. Two lines were used for the analysis of this isotope, both showing a good agreement with NDS as far as their relative intensities were concerned. The time evolution characteristics of the lines, though not of an excellent quality, were acceptable. One other note of relevance is the fact that each of the lines used for the analysis had a small admixture from the ground/metastable states. This could also contribute towards the slightly higher yields in each case. In this case much better agreement was observed with the Studsvik $^{90}Rb^g$ yield.

Seven gamma lines were used in the analysis of $^{96}Y^m$, all having excellent agreement with the NDS lifetime and relative gamma-ray branching ratios. The present study was not sensitive to $^{96}Y^g$ transitions. NDS [16] quotes two experiments, one in 1975 [17] and the other in 1987 [18], on which the $^{96}Y^m$ level scheme, branching ratios, etc. are based. Both the experiments agree well with each other, so the NDS values for the branching ratios do not appear to be suspect. Our independent yield for $^{96}Y^m$ is approximately half of the ^{96}Y ENDF value. If the ENDF value is assumed to be the total yield for ^{96}Y (metastable+ground), then our measured value for the metastable state suggests an approximately equal strength for the unmeasured ground state yield.

For ^{97}Y and ^{100}Y ENDF/B-VI does not list a metastable state, although NDS does indicate an isomeric state in each case. If our experimental values of the yields for the metastable and the ground state are added up in the case of ^{97}Y, the total yield is seen to be in excellent agreement with the ENDF value. In the case of ^{100}Y, for which only the ground state independent yield was experimentally determined, the experimental value is very close to half the ENDF value. This seems to indicate that the ENDF assignment is for the total yield and it appears that the ground and metastable yields are nearly equal. Note also that ENDF assigns a high uncertainty for the ^{100}Y independent yield. The independent yield of the metastable state could not be determined in the present study due to a lack of absolute intensity information of the gamma lines associated with this isomer in NDS.

For $^{99}Nb^m$ the experimental value of the yield is higher than the ENDF value by an order of magnitude. In this case five lines were seen, out of which two were chosen for the yield analysis. However, even the weaker lines that were not chosen had the correct relative intensities. In this case no obvious explanation can be presented for the discrepancy, but some possible reasons are outlined in the next paragraph.

The metastable and the ground states of ^{99}Nb are fed by ^{99}Zr which itself has a high yield. In deducing the independent yield of the daughter, this contribution was peeled-off by the procedure explained in the preceding section. If the branching ratios (of the feeding from the parent, ^{99}Zr) to metastable and ground states of ^{99}Nb are in error, our independent yield for each state would change significantly. Another possibility could be an overestimated ground-state beta branch in the decay of $^{99}Nb^m$ to ^{99}Mo by the NDS (the data sheets indicate a 65% beta branch going to the ground state for this first forbidden $1/2^-$-$1/2^+$ transition, which seems unusually high).

Discrepancies other than those involving isomeric states will now be considered. For the case of ^{89}Rb four gamma transitions were used, all with energies >1 MeV, with proper intensities and time behavior. The higher independent yield of ^{89}Rb could be attributed to an NDS overestimation of the ground-state beta branch. However, even a value of 0% for this branch, instead of 25% as assumed by the NDS,

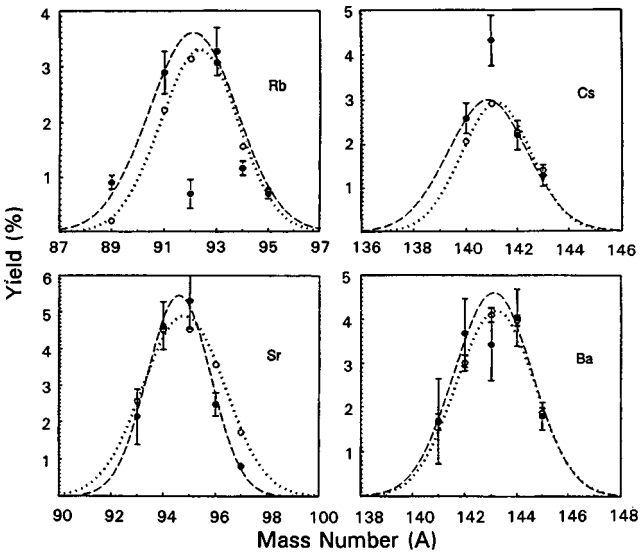

FIG. 5. Comparison of the independent yields of isotopes of Rb, Sr, Cs, and Ba. The abscissa represents the mass number and the ordinate is the percent independent yield. Dashed and dotted curves are drawn to guide the eye along the expected Gaussian distribution of independent yields for a given fixed atomic number.

TABLE IV. Comparison of cumulative yields (and their percentage uncertainties).

Isotope	$t_{1/2}$	ENDF	Expt.	Rudstam	Expt./ENDF	Expt./Rudstam
^{89}Rb	15.2 m	4.716 (1.4)	5.39 (3)	6.23 (8)	1.14 (3)	0.87 (9)
^{90}Rb^{g}	2.55 m	4.499 (1.4)	4.9 (13)	5.49 (9)	1.09 (13)	0.89 (16)
^{90}Rb^{m}	4.3 m	1.24 (45)	2.18 (9)		1.76 (46)	
^{91}Rb	58.4 s	5.577 (1)	6.28 (6)	5.25 (5)	1.13 (6)	1.20 (8)
^{92}Rb	4.5 s	4.18 (16)	7.4 (11)	4.72 (9)	1.8 (19)	1.57 (14)
^{93}Rb	5.7	3.551 (1)	3.7 (11)	3.72 (7)	1.04 (11)	0.99 (13)
^{93}Sr	7.42 m	6.238 (1)	6.0 (14)	5.4 (17)	0.96 (14)	1.11 (22)
^{94}Rb	2.7 s	1.649 (3)	1.25 (10)	1.31 (9)	0.76 (10)	0.95 (14)
^{94}Sr	1.25 m	6.063 (1.4)	5.8 (12)	5.9 (14)	0.96 (12)	0.98 (18)
^{95}Rb	0.38 s	0.770 (4)	0.70 (13)	0.71 (7)	0.91 (14)	0.99 (15)
^{95}Sr	25.1 s	5.271 (1.4)	6.0 (13)	5.19 (5)	1.14 (13)	1.16 (14)
^{96}Sr	1.06 s	3.756 (2)	2.6 (13)	3.9 (18)	0.69 (13)	0.67 (22)
^{96}Y^{m}	9.6 s	2.02 (45)	0.94 (11)		0.46 (46)	
^{97}Sr	0.42 s	1.749 (3)	0.84 (14)	2.63 (20)	0.48 (14)	0.32 (24)
^{97}Y^{g}	3.5 s	4.89 (23)	2.1 (17)		0.86[a] (26)	
^{97}Y^{m}	1.23 s		2.1 (13)			
^{98}Y^{g}	0.64 s	1.92 (23)	1.45 (13)		0.75 (26)	
^{98}Y^{m}	2.0 s	1.11 (32)	1.6 (22)		1.4 (39)	
^{99}Y	1.47 s	2.083 (6)	1.36 (17)		0.65 (18)	
^{99}Zr	2.1 s	5.63 (11)	4.6 (21)		0.82 (24)	
^{99}Nb^{m}	2.6 m	2.096 (4)	6.7 (15)		3.2 (16)	
^{100}Y^{g}	0.74 s	0.61 (64)	0.25 (22)		0.4 ($>$68)	
^{100}Zr	7.1 s	5.58 (32)	4.3 (15)		0.77 (35)	
^{101}Zr	2.1 s	3.071 (3)	3.2 (11)		1.04 (11)	
^{102}Zr	2.9 s	2.05 (11)	4.2 (12)		2.0 (16)	
^{136}I^{g}	1.39 m	2.643 (6)	2.5 (15)	3.9 (21)	0.95 (16)	0.64 (26)
^{136}I^{m}	46.9 s	1.264 (6)	1.07 (15)		0.85 (16)	
^{140}Cs	1.06 m	5.745 (1.4)	6.27 (6)	4.3 (12)	1.09 (6)	1.46 (13)
^{141}Cs	24.9 s	4.169 (1.4)	5.6 (10)	4.28 (11)	1.34 (10)	1.31 (15)
^{141}Ba	18.27 m	5.829 (3)	7.2 (15)		1.23 (15)	
^{142}Cs	1.7 s	2.717 (3)	2.6 (13)	2.69 (12)	0.96 (13)	0.97 (18)
^{142}Ba	10.6 m	5.753 (2)	6.4 (13)		1.11 (13)	
^{143}Cs	1.78 s	1.455 (3)	1.3 (19)	1.41 (18)	0.89 (19)	0.92 (26)
^{143}Ba	14.5 s	5.545 (3)	4.8 (18)	7.3 (12)	0.87 (18)	0.66 (22)
^{143}La	14.1 m	5.925 (3)	7.6 (18)		1.28 (18)	
^{144}Ba	11.4 s	4.396 (2)	4.4 (15)	4.36 (11)	1.00 (15)	1.01 (19)
^{144}La	40.9 s	5.465 (1.4)	4.8 (28)		0.88 (28)	
^{145}Ba	4.31 s	1.933 (6)	1.9 (17)	2.34 (25)	0.98 (18)	0.81 (30)
^{145}La	24.8 s	3.848 (4)	5.6 (24)		1.46 (24)	
^{146}La	6.27 s	2.411 (4)	2.2 (14)		0.91 (15)	
^{147}La	4.4 s	0.889 (6)	1.9 (17)		2.1 (18)	

[a]Metastable and ground state yields added up since ENDF/B-VI does not list the metastable state contribution.

would lower our deduced value by only 25%, still well above the ENDF value. It should be noted that the value quoted by the Studsvik group is also quite high compared to the ENDF value.

In the determination of the independent yield of ^{92}Rb we have chosen to use the gamma line intensities from Rudstam *et al.* [9] instead of the NDS due to the following considerations. On using the gamma intensities from NDS, the independent yield for this isotope was found to be anomalously low. This may be due to an underestimation of the ground-state beta branch value by the NDS. In fact NDS cautions about using this value for calculating the gamma intensities [19]. Though the beta branch value chosen by the NDS evaluators for the ground state is 51% (based on beta decay systematics) NDS also quotes an experimental value of 94% for this branch [20], which they have chosen to ignore on the basis of the resulting log *ft* value. One more reason for expecting a higher value for the yield arises from the nature of the yield distribution in Fig. 5. This figure shows a plot of the independent yields (our values and ENDF) for four elements as a function of the isotope mass number. It can be seen quite clearly that if the Gaussian distribution model is true, which generally seems to be the case, the independent yield for ^{92}Rb should be near the ''top'' of Gaussian curve,

in other words, significantly higher than the measured value. From the Gaussian curve, the value of our independent yield for ^{92}Rb should have been about 3.6%. This value of the independent yield is consistent with a beta branch of ~90% to the ground state of the daughter, ^{92}Sr. Since the Gaussian model works quite well in the cases examined here, it would seem that the proper beta branch to the ground state may very well be nearly 90%, in good agreement with the experimental result of 94% given in [20]. These considerations lead us to choose in this case the line intensities as listed in [9] and presumably taken from [20] rather than those of the NDS since the former are consistent with the 90% ground state beta branch suggested by the yield systematics. With this choice our resulting experimental value is somewhat higher than the ENDF value.

Our experimental yields of ^{94}Rb, ^{96}Sr, and ^{97}Sr are much lower than the ENDF values. In each case a sufficient number of lines, all showing the expected temporal characteristics and intensities were used. There does not seem to be a clear cut explanation for the discrepancies.

The high experimental value of ^{102}Zr is probably the result of basing the yield analysis on a single gamma line. The confidence level in this value is thus not as high as in the other cases and our deduced value should be accepted with caution.

For the case of ^{141}Cs, the NDS indicate a beta branch of 57% to a 55-keV level in the daughter [21]. This is also the dominant branch in the level scheme, while the beta branches to all other excited levels are one or two orders-of-magnitude lower. Thus an overestimation of the beta branching ratio to the 55-keV level could have easily resulted in the observed high experimental yield.

In the case of ^{143}La, four lines, all with the proper time and intensity behavior were used. The NDS indicate a near-zero ground state branch. There is no obvious reason for the anomalously high yield determined in this experiment. It should also be pointed out that both the experimental and ENDF values have high uncertainties. The relatively high uncertainty in the experimental yield of ^{143}La arises due to the fact that its precursor, ^{143}Ba, itself has a large independent yield which was subtracted from the observed yield of ^{143}La to deduce the independent yield.

For ^{144}La the six lines used were all in agreement with the NDS as far as the relative intensities and time evolution were concerned. However, the NDS comments indicate that there may be more high energy levels (>2 MeV) in the energy level scheme of this isotope [22]. If that is the case, then the present beta branching ratios are improperly normalized, giving a low experimental yield despite the good agreement in the relative intensities of the individual lines.

For ^{145}La several lines all in excellent agreement with NDS were used. However, one particular gamma line of 0.7865 MeV which was not used in the analysis had an intensity nearly ten times the value quoted in NDS. This anomalous result suggests a possible problem with the NDS absolute gamma-ray intensities of ^{145}La used in our analysis. In the case of ^{147}La only two lines were used for the analysis, so the experimental value should be accepted cautiously.

Cumulative yields

Table IV lists our experimental cumulative yields of isotopes and the equivalent values from ENDF/B-VI. The calculation of cumulative yields of rubidium and cesium isotopes needs some comments. As mentioned earlier, the cumulative yields were calculated according to Eq. (2). However, krypton and xenon (precursors of rubidium and cesium respectively) being noble gases, diffused quickly from the transport tape and were not detected in this study. As a result, their independent yields could not be measured experimentally. The values of the independent yields of the krypton and xenon isotopes [which had to be substituted in Eq. (2) for calculating the cumulative yields of rubidium and cesium isotopes] were hence taken from the ENDF/B-VI compilation.

Charge and mass complements

Since almost all fission events ($\geqslant$99%) result in two fragments, it may be useful to estimate the unmeasured yield of an isotope if the yield of its complement has been experimentally determined. Consider the following fission process:

$$^{235}\mathrm{U}+n\rightarrow{}^{A}X_{z}+{}^{(236-A)}Y_{(92-Z)},$$

which results in two fragments (X and Y, called comple-

TABLE V. Comparison of partial and total elemental yields (and their percentage uncertainties). The percentage of the total yield measured in this experiment is indicated within square brackets next to each element.

Element	Partial yield ENDF	Partial yield Expt.	Expt./ENDF	Total yield ENDF	Total yield Expt.	Expt./ENDF
Rb[a] [72]	8.67 (5)	11.1 (6)	1.28 (8)	12.04 (4)	14.5 (6)	1.20 (7)
Sr [88]	16.91 (1)	15.4 (8)	0.91 (8)	19.28 (1)	17.7 (8)	0.92 (8)
Y[b] [71]	8.83 (15)	7.2 (7)	0.82 (17)	12.37 (12)	10.7 (7)	0.87 (14)
Zr [74]	13.13 (14)	14.1 (9)	1.07 (17)	17.76 (12)	18.8 (9)	1.06 (15)
Cs [79]	8.67 (2)	10.4 (7)	1.20 (7)	10.78 (2)	12.5 (7)	1.16 (7)
Ba [89]	14.62 (2)	14.6 (11)	1.00 (11)	16.36 (3)	16.4 (11)	1.00 (11)
La[c] [85]	5.12 (4)	7.0 (26)	1.37 (26)	6.04 (7)	9.0 (26)	1.49 (27)

[a]Excluding the independent yield of ^{92}Rb.
[b]Excluding the independent yield of ^{98}Y^{m}.
[c]Excluding the independent yield of ^{143}La.

TABLE VI. Comparison of total elemental yields (and their percentage uncertainties) estimated on the basis of charge complementarity.

Element	ENDF	Estimated	Est./ENDF
Cs	10.78 (2)	14.5 (6)	1.35 (7)
Xe	20.04 (5)	17.7 (8)	0.88 (10)
I	11.55 (3)	10.7 (7)	0.93 (8)
Te	17.29 (3)	18.8 (9)	1.09 (10)
Rb	12.04 (4)	12.5 (7)	1.04 (8)
Kr	15.58 (1)	16.4 (11)	1.05 (11)
Br	5.25 (3)	9.0 (26)	1.7 (27)

ments) having the indicated atomic charge and mass. Each fragment may give off prompt neutrons following the fission process. The number of prompt neutrons ''boiled off'' by each fragment varies and has a near Gaussian distribution about an average (most probable) value. The average number of prompt neutrons emitted by fission fragments to form a product of a fixed mass is roughly between 1 to 1.5 for the isotopes measured in this experiment [15]. If this number is taken to be 1, to a first approximation, then the two fission products that are formed after prompt neutron emission are $^{(A-1)}X_z$ and $^{(235-A)}Y_{(92-Z)}$. Thus if charge and mass complementarity are assumed to hold good, measurement of the yield of one of the isotopes, say $^{(235-A)}Y_{(92-Z)}$, is enough to predict the yield of its complement, $^{(A-1)}X_z$. Of course the approximation that only 1 neutron is given out by each fragment may not be justified at all times. Hence predicting the yield of the complement in each case, using this approach, is only an estimate. Since charge conservation is a more dependable assumption, a better method is to add up the independent yields of all the isotopes of a fixed element (Z = const) and use that information to deduce the elemental yield of its charge complement $(92\text{-}Z)$.

Due to the gamma-ray sensitivity level of this experiment not all the isotopes of any one given element were measured. Typically isotopes with independent yields $<0.5\%$ were not observed, or in some cases, the measured yield of a certain isotope was suspect (e.g., ^{143}La). Excluding these, the measured independent yields of all the isotopes of a particular element were added to estimate the partial elemental yield. The independent yields of the excluded isotopes were taken from ENDF/B-VI and added to this partial sum so as to estimate the total independent yield for each element. Table V shows the values of the experimentally measured partial and total elemental yields and the equivalent ENDF values. The agreement is seen to be quite good except for La which as discussed earlier has several isotopes whose NDS gamma-ray intensity values are questionable. Table VI is a list of the *estimated* total elemental yields based on charge complementarity, from the values in Table V. The ENDF values were calculated by adding the independent yields of the complements of each measured isotope. Again, the agreement is good except in the case of Br, which is due to the fact that our value for its complement (La) is also on the higher side. In general it seems that charge complementarity is fairly reasonable way of estimating unknown elemental yields if the complementary yields are experimentally measured.

Figure 6 is a plot of the experimental values of the total

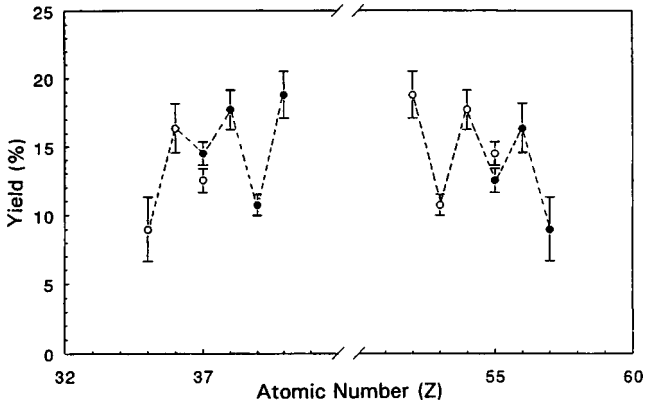

FIG. 6. Even-odd effect in the distributions of total elemental yields. Solid circles: measured values; open circles: estimated values from charge complementarity.

elemental yields. The solid circles represent the measured values and the open circles denote the estimated values based on charge complementarity. The even-odd effect (relative enhancement of the even-Z yields compared to the odd-Z ones) is clearly evident. The case of Rb ($Z=37$) and Cs ($Z=55$) needs a special mention. The partial elemental yields for both these elements were measured experimentally and a correction made to account for the unmeasured isotopic yields, to estimate the total yield. On the graph, these values are shown along with the values as predicted by complementarity. As seen, both the values are in good agreement with each other, implying that charge complementarity is indeed a reasonable way of estimating unmeasured elemental yields.

Although not as rigorous, the principle of charge-mass complementarity was used to estimate the yield of the metastable state of ^{98}Y. Even though the gamma lines associated with the beta decay of $^{98}Y^m$ could be seen, the independent yield for this isotope was calculated to be less than zero (after the subtraction of precursor contribution). The yield of ^{136}I (the heavy mass complement of ^{98}Y) was experimentally measured to be 2.28%. From complementarity, the total yield of ^{98}Y(metastable+ground) should be equal to this value to a first approximation. Since the independent yield for $^{98}Y^g$ was experimentally determined to be 1.44%, this allowed us to estimate an independent yield of 0.83% for $^{98}Y^m$, which we have adopted and included in Table III.

Gaussian distribution of yields

Figure 5 shows the distribution of independent yields for four elements. The solid circles denote the experimentally measured yields while the open circles represent the ENDF values. Dashed and dotted Gaussian curves are drawn (ignoring the even-odd effect) merely to guide the eye along the expected distribution. These curves are not representative of any kind of curve-fitting routine used in conjunction with the actual data and have been drawn to approximately estimate any trends that may be seen. The yields of ^{92}Rb and ^{141}Cs are markedly off from the Gaussian curves and the possible reasons for these discrepancies were already discussed in the prior section. In general the trend of independent yields to have a near-Gaussian distribution is sufficiently clear.

There are some differences between the widths of the measured and ENDF distributions. For Rb and Cs the width

of our distributions is about 15% larger, for Ba it matches with the ENDF width and for Sr the experimental width appears to be about 25% narrower than that of the corresponding ENDF fit. Also, for Rb and Sr the width of the ENDF Gaussians are within 5% of each other. The difference in widths is about 10% for Cs and Ba. The experimental data indicate a 40% difference between the Rb and Sr widths and 5% between those of Cs and Ba. Our data thus indicate a fairly different width for each of the light mass elements but a similar width for the heavy mass elements. ENDF on the other hand, seems to indicate a near-equal width within both regions. These numbers should be taken in a qualitative sense because the curves are drawn only to help visualize the shape of the distribution.

V. CONCLUSION

The advantage of using a helium-jet/tape transport type system is the facility of measuring yields of short-lived fission products. The accuracy and reliability of the yield data are dependent to large extent on the correctness of information such as the beta branching ratios and gamma line intensities as tabulated in the Nuclear Data Sheets. Cases where this spectroscopic information is not well-known or is partially missing, can show a deviation from the expected results. Many of the discrepancies noted between the measured yields and ENDF/B-VI values have been attributed to incorrect spectroscopic data. An example is the case of ^{92}Sr whose yield should have been much higher (as indicated by its large deviation from the Gaussian distribution) than the one measured experimentally. Also, a number of the lanthanum yields suggest problems with the gamma-ray intensity data.

On the other hand, for the majority of isotopes which have well established spectroscopic information, the results provide accurate fission yields. It is noteworthy that 56% of the present yields are within 1σ of the ENDF/B-VI values. Furthermore, the fact that there is no systematic elemental discrepancy in yields supports the conclusion of our earlier x-ray study regarding the uniform elemental transfer efficiency of the helium-jet system. Of particular importance are the results for isotopes having both metastable and ground states, where ENDF/B-VI does not have a reliable way of splitting the yield in the proper ratio. A significant example is that of the $^{96-98}$Y isotopes, where ENDF has either ignored the metastable state (^{96,97}Y) or estimated equal yields for the metastable and ground state (^{98}Y). The present measurements have determined all three metastable yields and two of the three ground-state yields.

In addition, the relative enhancement of the even-Z yields compared to the odd-Z yields is clearly seen. Furthermore, the present study confirms that for a given element the yield distribution as a function of mass number follows a Gaussian form. In fact systematics suggest that significant deviation of a yield from the Gaussian shape is reason to question the validity of the gamma-ray intensity data used to deduce the yield value. Also, systematics of this study suggest that the widths of the Gaussian distributions vary for the light mass elements and are nearly constant for those in the heavy mass region. It was also demonstrated that charge complementarity is a useful way of estimating unmeasured elemental yields.

[1] T. R. England, W. B. Wilson, B. F. Rider, C. W. Reich, F. M. Mann, R. E. Schenter, M. C. Brady, and J. Katakura, Los Alamos National Laboratory Report LA-11972-PR (1990), p. 96.

[2] G. Rudstam and T. England, Los Alamos National Laboratory Report LA-11909-MS (1990).

[3] C. W. Reich, in *Proceedings of Specialists Meeting on Data for Decay Heat Predictions*, Studsvik, Sweden, 1987 (OECD, Paris, 1987), p. 107.

[4] K. Tasaka, J. Katakura, and T. Yoshida, in *Proceedings of the International Conference on Nuclear Data for Science and Technology*, Mito, Japan, 1988 (Saikon, Tokyo, 1988), p. 819.

[5] T. R. England and B. F. Rider, in *Proceedings of Specialists Meeting on Fission Product Nuclear Data*, Tokai, Japan, 1992 (OECD, Paris, 1992), p. 346.

[6] J. K. Dickens and J. W. McConnell, Phys. Rev. C **23**, 331 (1981).

[7] J. K. Dickens and J. W. McConnell, Phys. Rev. C **24**, 192 (1981).

[8] J. K. Dickens and J. W. McConnell, Phys. Rev. C **27**, 253 (1983).

[9] G. Rudstam, P. Aagaard, B. Ekström, E. Lund, H. Göktürk, and H. U. Zwicky, Radiochim. Acta **49**, 155 (1990).

[10] R. S. Tanczyn, G. P. Couchell, and W. A. Schier, Comput. Phys. Commun. **39**, 61 (1985).

[11] P. R. Bennett, W. A. Schier, G. P. Couchell, E. S. Jacobs, D. J. Pullen, and M. F. Villani, Nucl. Instrum. Methods Phys. Res. A **369**, 263 (1996).

[12] H. Feldstein and S. Amiel, Nucl. Instrum. Methods **113**, 181 (1973).

[13] T. R. England, W. B. Wilson, and M. G. Stamatelatos, Los Alamos National Laboratory Report LA-6745-MS, also published as EPRI NP-356, Part 1 (1976).

[14] T. R. England, W. B. Wilson, and M. G. Stamatelatos, Los Alamos National Laboratory Report LA-6745-MS, also published as EPRI NP-356, Part 2 (1976).

[15] A. C. Wahl, At. Data Nucl. Data Tables **39**, 1 (1988).

[16] L. K. Peker, Nucl. Data Sheets **68**, 193 (1993).

[17] G. Sadler *et al.*, Nucl. Phys. **A252**, 365 (1975).

[18] M. Stolzenwold, G. Lhersonneau, G. Menzen, and K. Sistemich, JUL-Spez-403 (1987), p. 18.

[19] C. M. Baglin, Nucl. Data Sheets **66**, 369 (1992).

[20] R. J. Olson, W. L. Talbert, Jr., and J. R. McConnell, Phys. Rev. C **5**, 2095 (1972).

[21] L. K. Peker, Nucl. Data Sheets **45**, 65 (1985).

[22] J. K. Tuli, Nucl. Data Sheets **56**, 642 (1989).